Materials Chemistry and Physics 110 (2008) 387–392

Contents lists available at ScienceDirect

Materials Chemistry and Physics

journal homepage: www.elsevier.com/locate/matchemphys

Effect of aging on the properties of mesoporous niobium oxide

Sirachaya Kunjara Na Ayudhya, Apinan Soottitantawat, Piyasan Praserthdam*, Chairit Satayaprasert

Center of Excellence on Catalysis and Catalytic Reaction Engineering, Department of Chemical Engineering, Faculty of Engineering, Chulalongkorn University, Bangkok 10330, Thailand

ARTICLE INFO

Article history:
Received 6 December 2007
Received in revised form 18 February 2008
Accepted 21 February 2008

Keywords:
Aging
Niobium oxide
Mesoporous
Nanostructures

ABSTRACT

Using niobium(V) chloride and F127 in a water–ethanol system, this work reports the effect of aging of niobium-surfactant gel at 40 and 110 °C on the final product properties. The aging at low temperature of 40 °C showed small modification of the textural properties of the mesoporous niobium oxide. On the other hand, the hydrothermal aging at 110 °C showed significant increase in BET surface area, pore volume, pore size and microporosity with additional thermal and structural properties deviation. The process of hydrothermal aging at 110 °C is believed to lock chlorides in the niobium structure and cause the structural modification of the niobium skeleton leading to distinct developed crystalline structure and phase transformation behavior. The result also showed that hydrothermal aging at 110 °C could also enhance Lewis acidity of the product after calcination at 500 °C.

1. Introduction

Nanoporous niobium oxide is one of transition metal oxides expected to be applicable in catalysis, electronic, sensing devices, and biotechnology [1–5]. Among important properties, high surface area is crucial for catalyst supports, photocatalysts [1,6–8] while large pore size is also crucial for applications as adsorbents and sensors [2].

Synthesizing niobium oxide without surfactant generally resulted in low surface area oxide. For example, Suh and Park [9] mixed niobium(V) ethoxide with methanol and nitric acid and obtained niobium oxide with surface area of 26 $m^2 g^{-1}$ after calcination at 500 °C for 2 h. Ikeya and Senna [10] showed an amorphous niobium oxide having surface area of only 10 $m^2 g^{-1}$ after heating at 380 °C for 3 h. The niobium oxides possessing high surface area were obtained by adding surfactant template in the synthesis processes. Pluronic P123 ($EO_{20}PO_{70}EO_{20}$, EO = ethylene oxide, PO = propylene oxide) triblock copolymer and niobium(V) chloride were employed to get the mesoporous niobium oxide having surface area of 196 $m^2 g^{-1}$ after calcination at 400 °C in the work of Yang et al. [4] and surface area of 84 $m^2 g^{-1}$ after calcination at 500 °C in the work of Chen et al. [7]. Lee et al. [11] employed Pluronic P85 and got surface area of 210 $m^2 g^{-1}$ after calcinations at 450 °C. The mesopores of these samples were generated from removal of the surfactant and usually ranged at 4–5 nm for the samples having surface area of more than 150 $m^2 g^{-1}$.

It was known that the BET surface areas and the pore volumes of the mesoporous samples decrease with an increase of the calcination temperature [7,8]. Therefore, the inability to withstand high temperature is a serious limitation for most catalysis applications [12]. Crystallization of an inorganic phase, which grows beyond the wall thickness and deteriorate the mesostructure could account for a relatively low stability to thermal treatment of mesoporous oxides [13]. An incomplete condensation of the inorganic network also resulted in destruction of the mesostructure [14].

In sol–gel chemistry, aging could enhance the strength and stiffness of the gel. The more and more inorganic species were hydrolyzed and added to the wall structure yielding a less-shrinked gel. A greater pore size and pore volume of the dried gel were obtained [15]. For the template assisted system, aging the as-prepared mesostructured hybrid prior to calcination not only permits a better consolidation of the inorganic walls [12] but also change template shape and size, and hence the pore size, surface area and porosity of the final products. For instances, in mesoporous silica SBA-15 materials, hydrothermal aging the as-prepared precipitates in the mother liquors at 80–100 °C resulted in larger surface area, pore volume and pore size [16]. In the work of Kim et al. [17], mesoporous silica synthesized with P123 also showed an increase of surface area and pore size when aged at 120 °C. The effect of aging on the silica based system has been widely investigated while relatively little information has been presented on the aging effect of transition metal oxides gel on the textural properties [18]. In the case of porous niobium oxide, Lee et al. [19] showed that the second step aging in an open atmosphere at 100 °C after initial aging at 40 °C could help stabilizing the niobium wall but resulted

* Corresponding author.
E-mail address: piyasan.p@chula.ac.th (P. Praserthdam).

0254-0584/$ – see front matter © 2008 Elsevier B.V. All rights reserved.
doi:10.1016/j.matchemphys.2008.02.027

Table 1
Characterization results of the samples calcined at 500 °C

Samples	BET specific surface area ($m^2\ g^{-1}$)[a]	Pore volume ($cm^3\ g^{-1}$)[b,c]	Average pore diameter (nm)[d]	*t*-plot micropore area ($m^2\ g^{-1}$)[e]	*t*-plot micropore volume ($cm^3\ g^{-1}$)[e]	% weight loss at crystallization[f]	Nb/Cl ratio[g]
d110	78	0.099	4.1	2.928	0.0005	2.1	44
d40–d110	91	0.120	4.1	6.307	0.0020	0.6	22
H40–d110	105	0.157	4.5	4.400	0.0009	0.6	17
H110–d110	151	0.252	5.4	9.732	0.0030	0.0	121

[a] ±10% error.
[b] Determined from the single point adsorption total pore volume of pores at $p/p_o \sim 0.99$.
[c] From BJH desorption.
[d] See pore size distribution in Fig. 1.
[e] The value of micropore area is obtained from subtraction of *t*-plot external surface area from the BET surface area. The *t*-plot calculations are based on the Harkins and Jura equation.
[f] From TGA in Fig. 2.
[g] From SEM-EDS.

in lower BET surface area after washing with water, compared to that of the sample aged only at 40 °C.

To our knowledge, there has been no report on hydrothermal aging of transition metal-template system and its effect on the final product properties. In this study, we have investigated the effect of the aging in an open atmosphere and aging in a close vessel (hydrothermal aging) on the properties of niobium oxide synthesized from niobium(V) chloride and triblock copolymer.

2. Experimental

2.1. Synthesis

First, the niobium precursor solution was made by mixing 8 mmol of niobium(V) chloride, $NbCl_5$ (99.9%, Aldrich) with 262 mmol of absolute ethanol (>99.9%, Merck) under argon atmosphere. Triblock copolymer $(HO(CH_2CH_2O)_{106}(CH_2CH(CH_3)O)_{70}(CH_2CH_2O)_{106}H$ (designated $EO_{106}PO_{70}EO_{106}$, F127, Aldrich) was dissolved in absolute ethanol and distilled water to make the polymer solution. The niobium and polymer solution were mixed to get the total molar ratio of Nb:water:ethanol:F127 at 1:37:51:0.0325 and then stirred for 16 h to make sure the complete mixing. These were done in room temperature (25–32 °C). The obtained solution was transparent. Then it would be directly dried on a Petri dish at 100–110 °C (in an oven) for 1 week or until it was dried for a non-aged sample. This sample is designated as d110.

For the sample aged in an open air at 40 °C, the material would be dried on a Petri dish at 40 °C for 24 h prior to drying at 110 °C, designated as d40–d110. For the hydrothermally aged samples, the material was put into a closed vessel and heated for 24 h (autogenious pressure) at 110 °C for the sample designated H110–d110 or at 40 °C for the sample designated H40–d110, before they were dried on a Petri dish at 100–110 °C (in an oven).

The dried samples were crushed into powder and calcined at 500 °C (or at other temperature if specified) for 5 h (1 °C min^{-1} ramp rate) to remove the polymer template.

2.2. Sample characterizations

The pre-calcined products were characterized by thermogravimetric analyzer-differential scanning calorimeter (TGA-DSC) and Scanning electron microscopy-energy dispersive spectrometer (SEM-EDS) while the calcined products were characterized by X-ray diffractometer (XRD) and nitrogen physisorption measurement. The TGA-DSC analysis was performed with an SDT Q600 instrument under oxygen flowing at 100 ml min^{-1} and heating rate of 5 °C min^{-1}. The SEM-EDS was performed on JEOL (JSM-6400 and JSM-5410LV). The powder X-ray diffractometer was performed by SEIMENS D5000, using CuKα radiation at 30 kV and 30 mA with a Ni filter. The nitrogen physisorption measurements were performed at 77 K using Micromeritics ASAP 2020.

3. Results and discussion

3.1. The effect of aging on the textural properties

Table 1 shows textural properties of the calcined products along with some of the results from the TG-DSC and the SEM-EDS. All samples showed IV type isotherm with hysteresis loop (Fig. 1a), which indicates the development of mesoporosity in the samples, and the mesopore volumes were significantly larger than the micropore volumes. Simple drying at 110 °C (the d110) gave the lowest BET specific surface area and pore volume. The consecutively increases in BET specific surface area and pore volume were observed for the aged samples: d40–d110, H40–d110 and H110–d110. The results of the *t*-plot micropore area and micropore volume also showed little higher microporosity of all the aged samples. The H110–d110 seemed to have highest BET specific surface area, pore volume and microporosity.

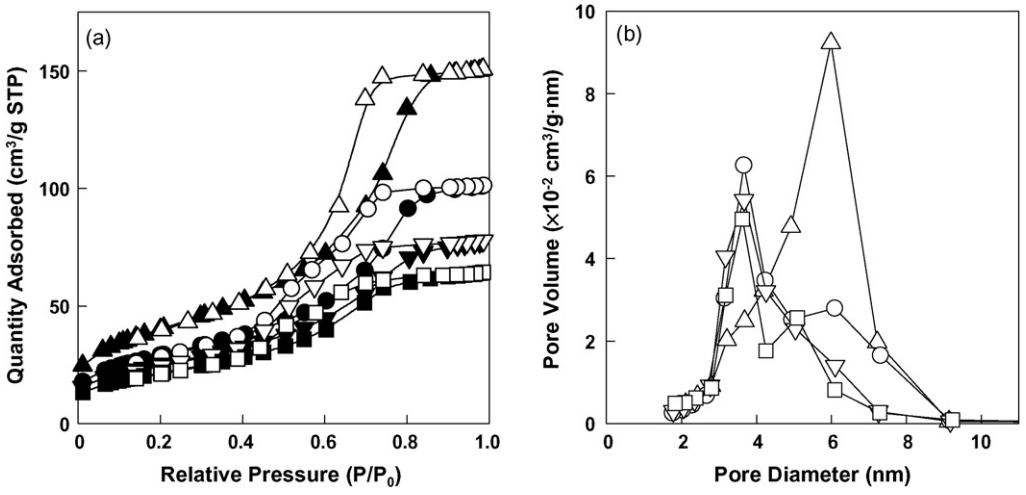

Fig. 1. Adsorption and desorption isotherms (a) and mesopore size distribution (b) of the samples calcined at 500 °C for 5 h (1 °C min^{-1}): (△) H110–d110, (○) H40–d110, (▽) d40–d110, (□) d110 (closed symbols: adsorption, open symbols: desorption).

The pore size distributions were shown in Fig. 1b. The sample directly dried at 110 °C (the d110) showed mainly the pore sizes centered at about 3.5 nm with an observable fraction of the larger pore size, which centered at 5 nm. Aging in an open air and hydrothermal aging at 40 °C both made the larger size pores more widely distributed towards larger sizes. Significant increase of the pore size could be observed for the sample hydrothermally aged at 110 °C (the H110–d110) whose main pore sizes were centered at 6 nm with fraction of the smaller size pores much reduced.

For the shifting of the pore size distributions observed, it seems that the fraction of the larger size pores were more flexible and more easily subjected to changes. The mesophase having higher chloride distribution in the molecular scale might be responsible for the more flexibility of the hybrid mesophase adjustment [20]. The more flexible hybrid suggests that the inorganic–organic interaction is not too strong and the micellization of the F127 could be easily achieved resulting in the large pore sizes of the final oxide products. The stronger interaction, in contrast, may interfere micellization and give only the small pore sizes arisen from the space formerly occupied by improper formed micelles. It was found that the smaller pore sizes are similar to the pore sizes obtained from the synthesis using the same condition but without block copolymer (Fig. 1S in supporting information). For aging at 40 °C, either on an open air or in the closed vessel, the shifting of the larger pore sizes to even larger size could be accounted from micellar expansion induced by ethanol evaporation at 40 °C [21], but the consequent drying at 110 °C should have more pronounced effect on the product pore size distributions and only small deviation was observed as shown in Fig. 1b.

The micellar expansion due to ethanol evaporation could also occur for the H110–d110. However, its significant increase of the pore sizes should arise from the property of EO moieties of the polymer template, which expel water and become less hydrophilic when the temperature is higher than 60 °C [22]. This tends to provide larger hydrophobic portion of the template aggregates and the inorganic condensation, which takes place ideally in the polar phase (the phase where EO moieties generally occupy), would extend out to occupy the space of the aggregate corona further away from the micelle core, leaving larger pore sizes when the template is burnt out [13].

The less hydrophilic properties of the EO part also reflects a weaker interaction between the organic and the inorganic (favorably attached to the hydrophilic EO moieties) and provides more mobility for the proper folding of the block copolymer giving the larger pore sizes of the final mesoporous products. This explains the noticeable reduction of the fraction of smaller size pores with an increase in the fraction of the larger size pores of this sample.

The increase in surface area even with an increase in average pore sizes can be ascribed to the microporosity generated by the aging [15]. Although the *t*-plot has an error and limitation to access the true microporosity [15,23], its results (Table 1.) showing larger microporosity for all the aged samples could be used to support the cause of the increase in surface area even with an increase in average pore size. The high temperature aging could dehydrate EO moieties and reduce microporosity generated by entanglement of the EO units in the inorganic wall [13], but microporosity generated from the modification of the inorganic species themselves could contribute to surface area increase. Aging can promote the hydrolysis and condensation of the inorganic framework and the strength and stiffness of the wet gel could be increased [15]. This could yield a tighten structure giving a small pore in the niobium wall [24]. The high aging temperature at 110 °C gave more remark on these effects than the low aging temperature. The H110–d110 showed up to 150 $m^2 g^{-1}$ BET surface area even with large pore sizes of 6 nm. A less-shrinked gel also provides a greater pore volume of the dried gel due to higher ability to withstand capillary pressure [15] and explains the observations that the pore volume is increased with the surface area.

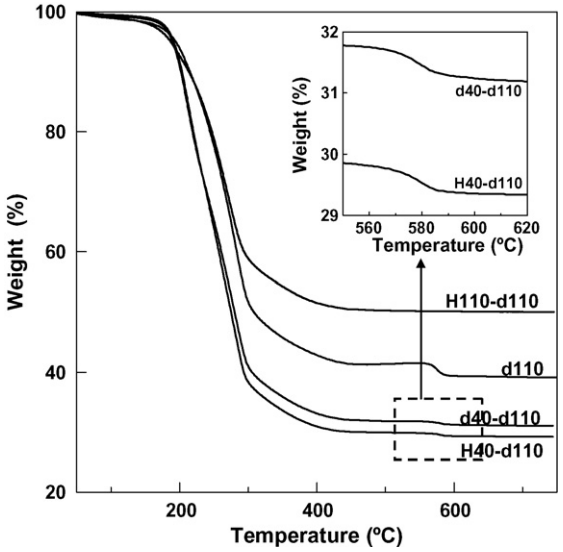

Fig. 2. TGA results of the pre-calcined samples. Inset is the enlargement of the weight loss of the d40–d110 and the H40–d110.

3.2. The effect of aging on the thermal and structural properties

The TGA-DSC showing the thermal behavior of the pre-calcined samples are shown in Figs. 2 and 3. In Fig. 2, all TGA curves show an initial slow loss of water below ~200 °C. More than 40% weight loss, corresponding to two main exothermic peaks in DSC curve in Fig. 3, was observed from ~180 to 300 °C. The minor exothermic peak occurred at ~180–250 °C could be the release of trapped water/ethanol or of HCl upon further movement of the inorganic network [20,25,26]. The presence of this minor exothermic peak probably depended on the amount of trapped HCl, which also contributed to the weight loss observed. The higher the amount

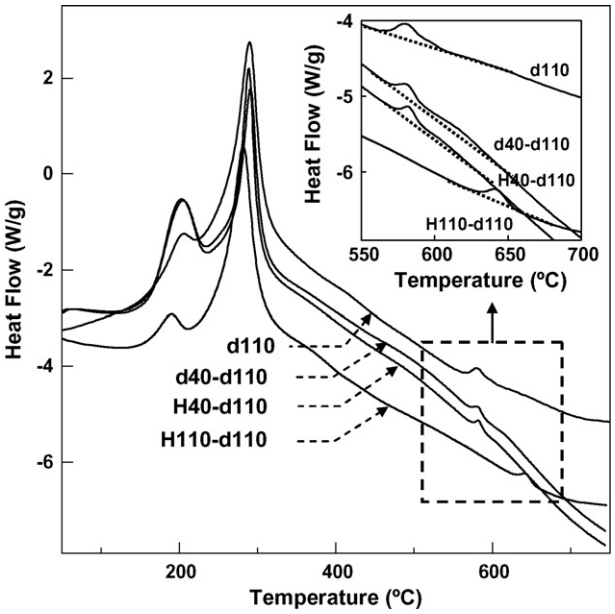

Fig. 3. DSC results of the pre-calcined samples. Inset is the enlargement of the crystallization peaks of all samples.

of Cl content (low Nb/Cl ratio detected by SEM-EDS) the higher the weight loss observed in TGA data. The main exothermic peak centered at ~280–290 °C, consistent with the large weight loss, is ascribed to main decomposition of the surfactant template [27–29]. This polymer decomposition shifted to lower temperature for the H110–d110 suggesting a little weaker bonding strength between niobium species and organic triblock copolymer of this sample [27]. The slow continuing weight loss after ~300–450 °C could be a release of volatile compounds that still trapped inside the pores or within the wall structure [25,30]. At the temperature ~580 °C, there is another small exothermic peak in the DSC curve for all the samples except for the H110–d110 of which this peak occurs at ~640 °C. These are attributed to crystallization of Nb_2O_5, which normally occurs above 500 °C for amorphous Nb_2O_5 [31]. The crystallization of the d110, d40–d110 and H40–d110 all started at ~580 °C and seemed to finish by the following small events at below 600 °C for the d110. The d40–d110 and H40–d110 showed a continuous crystallization event along the temperature up to ~650 °C, as shown by the blown out DSC in the inset of Fig. 3. The crystallizations occurred with weight loss for the d110 (non-aged sample; see Fig. 2) and the 40 °C aged samples (both the d40–d110 and the H40–d110; see the inset of Fig. 2) but not for the H110–d110. The percentages of weight losses observed at the crystallizations of each sample are given in Table 1.

The weight loss of 2.1% detected at crystallization for the non-aged sample (the d110) is in good agreement with the weight loss with HCl removal at more than 500 °C in the work of Schmitt et al. [26] and the 3 wt% removal of chloride detected in the work of Ikeya and Senna [10]. The weight loss detected at the crystallization was also observed for the non-aged alumina in the case of nonhydrolytic alumina gel using aluminum chloride as precursor, and it was proposed to be from chloride compound liberation [32]. Therefore, chloride should be responsible for the detected weight loss observed at the crystallization event for each sample in this work. The chloride here is believed to be the one that bonded to the niobium and required crystal structuring before being removed. It is different from the chloride presented as trapped HCl, which corresponded to the minor exothermic peak in the DSC data.

The non-aged sample (the d110) might contain larger amount of chloride bonded to the niobium, when compared to the H40–d110 and the d40–d110. The latter two samples showed only 0.6% weight loss at crystallization.It is presumed that the hydrolysis–condensation reaction was enhanced by the aging period resulting in lesser chloride content in the niobium structure but larger fraction of chloride dispersed in the system.

The fact that the H40–d110 and the d40–d110, when compared to the d110, showed longer tail of crystallization continuing along the higher temperatures suggests that the aging at 40 °C might provide more fraction of niobia having harder tendency to crystallize. It is presumed that more dispersed chloride could act as an impurity and prevent the crystallization of the oxide [33]. It is also possible that more entanglement of the block copolymer into the niobium wall could be responsible for this as its presence may prevent continuous structural arrangement of niobium oxide to form its crystallite structure. The d40–d110 showed a little longer tail of crystallization event than the H40–d110, probably because of more fraction of a less ordered molecular state might be generated while gellation occurred while aging in an open air at 40 °C.

For the H110–d110, its crystallization event occurred at much higher temperature when compared to the others. Besides, there was no detectable weight loss at its crystallization event. These may be related to the role of chloride that linked to the niobium and the high temperature aging condition that provided significant modification of niobia molecular structure.

It was known that chloride anions are able to form bridging in the niobium structure as a chloroalkoxide and still present after hydrolysis [10,34–36]. The role of chloride as complexing anion could change the positive charge of the metal atom and affect the metal–ligand bond strength leading to new molecular structure that exhibits new properties such as new chemical reactivity towards hydrolysis, condensation and new phase transition behavior [36]. Similar complexing ability was found in zirconia whose phosphate ligands are strong complexing anions able to act as bridging ligands and the existence of phosphate in the zirconia structure lead to higher crystallization temperature [37]. The hydrothermal aging at high temperature of 110 °C possibly enhanced chloride complexing ability making chloride incorporated ('locked') well in the niobium structure and created new organized molecular structure which exhibited much higher crystallization temperature.

The distinct molecular state of the niobium skeleton obtained from the hydrothermal aging at 110 °C could be supported by the crystal structure observed from the XRD. The XRD patterns of the samples after calcinations at 500 °C for 5 h (1 °C min^{-1}) are shown in Fig. 4a. The d110 (non-aged sample) showed an amorphous

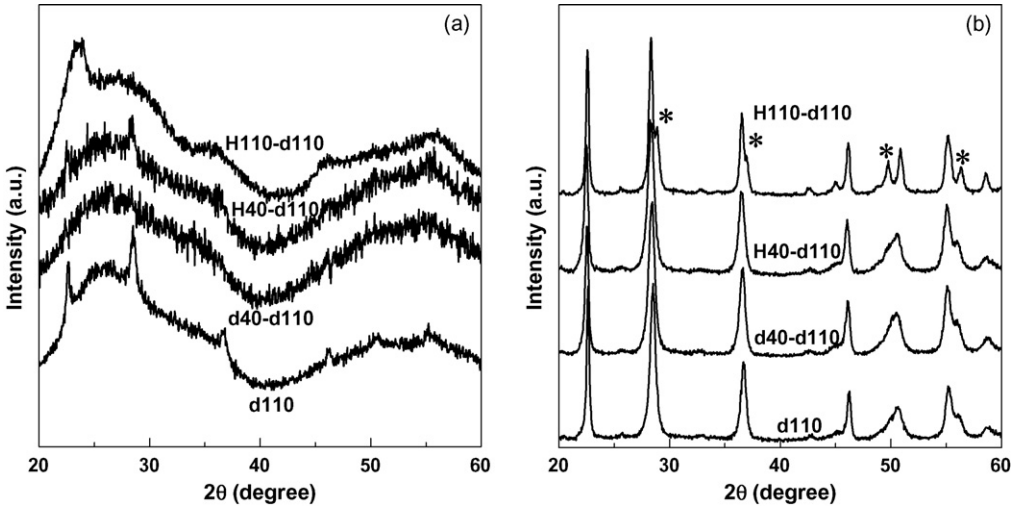

Fig. 4. XRD patterns of (a) the samples calcined at 500 °C for 5 h (1 °C min^{-1}); (b) the samples calcined at 600 °C for 5 h (1 °C min^{-1}). The splits in the pattern of an orthorhombic T-Nb_2O_5, which are distinguishable from a pseudohexagonal TT-Nb_2O_5 are indicated by the asterisks on the H110–d110 in (b).

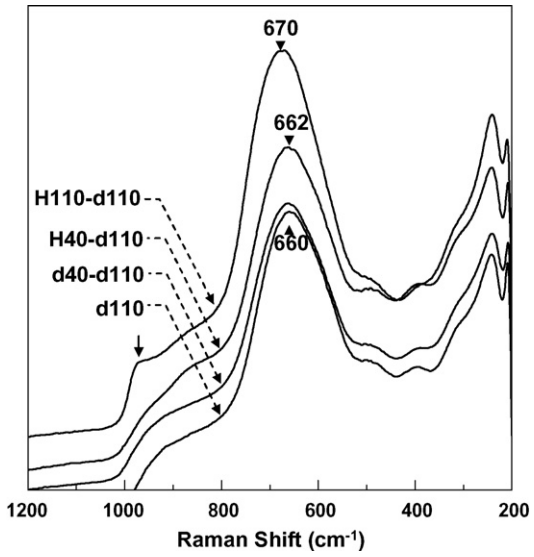

Fig. 5. Raman shifts of the samples calcined at 500 °C for 5 h (1 °C min^{-1}). The Raman band between 900 and 1200 cm^{-1} indicating the presence of Nb=O bonds in the highly distorted NbO_6 octahedra is pointed by the arrow.

characteristic with some evidence of crystallized structure whose pattern matches the pseudohexagonal Nb_2O_5 (TT phase: JCPDS 28-0317). The pattern of the H40–d110 and the d40–d110 also indicated a pseudohexagonal structure, similar to the d110, with more amorphous nature mainly shown in the d40–d110 sample. These are consistent to the DSC results in Fig. 3. For the H110–d110, its pattern showed mainly amorphous characteristic but with hidden growing structure whose pattern matches the tetragonal structure (JCPDS 18-0911) having maximum intensity at $2\theta \sim 23^\circ$ [38]. These imply different nature of the niobia derived from different aging conditions, especially the distinct developing pathway of the niobia synthesized under hydrothermal aging at 110 °C. When the samples were calcined at 600 °C (1 °C min^{-1}) (see Fig. 4b), only the H110–d110 showed an orthorhombic Nb_2O_5 (T phase) with crystalline structure matching JCPDS 30-0873 while all the other three samples clearly showed a fully crystallized pseudohexagonal Nb_2O_5 (TT phase).

The cause of the splits in the XRD pattern of the T phase were thought to be from some vacancies or monovalent species such as Cl^- that replace in some of the oxygen atoms positions of the normal pseudohexagonal TT structure [39]. The T phase was also found in the niobia obtained from high HCl content niobic acid in the work of Schafer et al. [31]. By recalling that an amorphous Nb_2O_5 possesses very similar features with the niobic acid [39], the phase transformation from an amorphous to an orthorhombic T structure of the H110–d110 should be induced by the chloride in the niobium structure.

Note that the obviously higher crystallization temperature and the T phase observed when the samples were subjected to hydrothermal aging at 110 °C is independent of the polymer type and whether the samples were synthesized with or without organic triblock copolymer (see Fig. 2S in supporting information).

Apart from the distinct crystallization behavior observed, the hydrothermal aging at 110 °C also showed exclusive Raman spectra. The Raman bands of all 500 °C-calcined samples were shown in Fig. 5. All samples have Raman bands in common at ~200–300 cm^{-1} which are angle deformation modes of Nb–O–Nb and bridging Nb–O–Nb bonds [40] and at ~600–700 cm^{-1} which should be slightly distorted NbO_7, NbO_8 group or slightly distorted NbO_6 possessing Nb–O bond with no non-bridging oxygen [39–41]. The Raman shift between ~800 and 900 cm^{-1} corresponding to a highly distorted NbO_6 [41] was also found in all samples. However, the high frequency Raman bands observed at ~900–1200 cm^{-1} seemed to predominantly occur only for the H110–d110. These bands and the shifting of the bands from 660 to 670 cm^{-1} indicates that appreciably distorted octahedra with a higher niobium–oxygen bond order (Nb=O bond) is present in the H110–d110 [42]. This Nb=O bonds in the highly distorted NbO_6 octahedra are associated with Lewis acid sites [39,43] indicating that after calcinations at 500 °C, the H110–d110 showed higher Lewis acidity than other samples. However, this strong Lewis acidity was not observed for the same sample after calcination at 600 °C when the structure has been changed into an orthorhombic and the Raman bands at ~900–1200 cm^{-1} disappeared.

It was believed in this work that the high temperature of the hydrothermal aging step that 'locked' the chlorides to stay cross-linked in the structure and withstand the liberation upon thermal treatment might presumably explain no detectable weight loss at the crystallization event of the H110–d110. These also lead to high crystallization temperature observed in DSC, the distinct phase transformation observed in XRD and to the outstanding Lewis acidity evidenced by the Raman.

4. Conclusions

This work shows that the aging could modify the textural, thermal and structural properties of the mesoporous niobium oxide synthesized by using niobium(V) chloride and F127 in a water–ethanol system. The aging at low temperature of 40 °C by dish drying and aging in a closed vessel showed small deviation of the pore size distributions, BET specific surface area, and pore volume from those of the non-aged sample. The surfactant micelle adjustment by different condition and the strengthened niobia network in the mesostructure wall due to an accelerated hydrolysis–condensation rate in higher temperature were used to account for the results observed. The hydrothermal aging condition at 110 °C showed exclusive properties. This sample showed highest BET surface area, pore volume, pore size, and microporosity. Also, it revealed distinctly high crystallization temperature, with no detectable weight loss. Chloride was proposed to be locked within the niobium structure under the step of hydrothermal aging at 110 °C, causing structural modification of the niobium skeleton to have distinct tetragonal phase at which an enhanced Lewis acidity was present and finally an orthorhombic crystalline structure after calcination at 600 °C.

Acknowledgements

This work was supported by the Thailand Research Fund (TRF). Also, the valuable point to discuss on the TGA-DSC results is acknowledged to Michael Grass from University of California, Berkeley.

Appendix A. Supplementary data

Supplementary data associated with this article can be found, in the online version, at doi:10.1016/j.matchemphys.2008.02.027.

References

[1] V.F. Stone Jr., R.J. Davis, Chem. Mater. 10 (1998) 1468.
[2] X. Xu, B. Tian, S. Zhang, J. Kong, D. Zhao, B. Liu, Anal. Chim. Acta 519 (2004) 31.
[3] S. Murray, M. Trudeau, D.M. Antonelli, Adv. Mater. 12 (2000) 1339.
[4] P. Yang, D. Zhao, D.I. Margolese, B.F. Chmelka, G.D. Stucky, Nature 396 (1998) 152.
[5] M.A. Bizeto, V.R.L. Constantino, Eur. J. Inorg. Chem. (2007) 579.

[6] U. Ciesla, F. Schuth, Micropor. Mesopor. Mater. 27 (1999) 131.
[7] X. Chen, T. Yu, X. Fan, H. Zhang, Z. Li, J. Ye, Z. Zou, Appl. Surf. Sci. 253 (2007) 8500.
[8] T. Ohuchi, T. Miyatake, Y. Hitomi, T. Tanaka, Catal. Today 120 (2007) 233.
[9] D.J. Suh, T.-J. Park, Chem. Mater. 8 (1996) 509.
[10] T. Ikeya, M. Senna, J. Mater. Sci. 22 (1987) 2497.
[11] B. Lee, D. Lu, J.N. Kondo, K. Domen, J. Am. Chem. Soc. 124 (2002) 11256.
[12] G. Soler-Illia, C. Sanchez, B. Lebeau, J. Patarin, Chem. Rev. 102 (2002) 4093.
[13] G. Soler-Illia, E.L. Crepaldi, D. Grosso, C. Sanchez, Curr. Opin. Colloid Interface Sci. 8 (2003) 109.
[14] M. Lindén, J. Blanchard, S. Schacht, S. Schunk, F. Schüth, Chem. Mater. 11 (1999) 3002.
[15] S. Smitha, P. Shajesh, P.R. Aravind, S.R. Kumar, P.K. Pillai, K.G.K. Warrier, Micropor. Mesopor. Mater. 91 (2006) 286.
[16] D. Zhao, Q. Huo, J. Feng, B.F. Chmelka, G.D. Stucky, J. Am. Chem. Soc. 120 (1998) 6024.
[17] K.D. Kim, G.B. Kim, H.T. Kim, J. Chem. Eng. Jpn. 38 (2005) 547.
[18] C.J. Brinker, G.W. Scherer, Sol–Gel Science: The Physics and Chemistry of Sol–Gel Processing, Acedemic Press, San Diego, 1989, pp. 358–373.
[19] B. Lee, D. Lu, J.N. Kondo, K. Domen, Chem. Lett. (2002) 1058.
[20] D. Grosso, G. Soler-Illia, F. Babonneau, C. Sanchez, P.A. Albouy, A. Brunet-Bruneau, A.R. Balkenenende, Adv. Mater. 13 (2001) 1085.
[21] K. Fontell, A. Khan, B. Lindström, D. Maciejewska, S. Puang-Ngern, Colloid Polym. Sci. 269 (1991) 727.
[22] C. Guo, H.Z. Liu, J.Y. Chen, Colloid Polym. Sci. 277 (1999) 376.
[23] S. Storch, H. Bretinger, W.F. Maier, Appl. Catal. A: Gen. 174 (1998) 137.
[24] L.C. Klein, Sol–gel Technology for Thin Films, Fibers, Preforms, Electronics and Specialty Shapes, Noyes Publications, New Jersey, 1988, p. 392.
[25] G. Soler-Illia, E. Scolan, A. Louis, P.A. Albouy, C. Sanchez, New J. Chem. 25 (2001) 156.
[26] M. Schmitt, S. Heusing, M.A. Aegerter, A. Pawlicka, C. Avellaneda, Sol. Energy Mater. Sol. Cell. 54 (1998) 9.
[27] B.L. Newalkar, S. Komarneni, Chem. Mater. 13 (2001) 4573.
[28] O. Metelkina, N. Hüsing, P. Pongratz, U. Schubert, J. Non-Cryst. Solids 285 (2001) 64.
[29] R.M. Grudzien, B.E. Grabicka, M. Jaroniec, J. Mater. Chem. 16 (2006) 819.
[30] G. Soler-Illia, C. Sanchez, New J. Chem. 24 (2000) 493.
[31] H. Schafer, R. Gruehn, F. Schulte, Angew. Chem. Int. 5 (1966) 40.
[32] G.S. Grader, Y.D. Hazan, D. Bravo-Zhivotovskii, G.E. Shter, J. Sol–Gel Sci. Technol. 10 (1997) 127.
[33] N. Kubota, Cryst. Res. Technol. 36 (2001) 749.
[34] M.A. Aegerter, M. Jafelicci Jr., D.F. Souza, E.D. Zanotto, Sol–gel science and technology, in: Proceedings of the Winter School on Glasses and Ceramics from Gels, World Scientific, Singapore, 1989, p. 142.
[35] C.L.T.d. Silva, V.L.L. Camorim, J.L. Zotin, M.L.R.D. Pereira, J.A.da.C. Faro, Catal. Today 57 (2000) 209.
[36] M.A. Aegerter, M. Jafelicci Jr., D.F. Souza, E.D. Zanotto, Sol–gel science and technology, in: Proceedings of the Winter School on Glasses and Ceramics from Gels, World Scientific, Singapore, 1989, pp. 72, 122, 142–156.
[37] U. Ciesia, M. Froba, G.D. Stucky, F. Schuth, Chem. Mater. 11 (1999) 227.
[38] P. Nair, J. Nair, A. Raj, K. Maeda, F. Mizukami, T. Okubo, H. Izutsu, Mater. Res. Bull. 34 (1999) 225.
[39] I. Nowak, M. Ziolek, Chem. Rev. 99 (1999) 3603.
[40] A.E. Lewandowska, M.A. Bañares, Catal. Today 118 (2006) 323.
[41] E.B. de Araujo, J.A.C. de Paiva, J.A. Freitas Jr., A.S.B. Sombra, J. Phys. Chem. Solids 59 (1998) 689.
[42] B.X. Huang, K. Wang, J.S. Churchb, Y.-S. Li, Electrochim. Acta 44 (1999) 2571.
[43] S.M. Maurer, E.I. Ko, J. Catal. 135 (1992) 125.